

The GRB Intrinsic Duration Distribution: Progenitor Insights Across Cosmic Time

NICOLE M. LLOYD-RONNING ,^{1,2} OMER BROMBERG ,³ AND TSVI PIRAN ,⁴

¹ *Computational Physics and Methods Group, Los Alamos National Lab, 87545, US*

² *Center for Theoretical Astrophysics, Los Alamos National Lab, 87545, US*

³ *The Raymond and Beverly Sackler School of Physics and Astronomy, Tel Aviv University, Tel Aviv 69978, Israel*

⁴ *Racah Institute of Physics, The Hebrew University, Jerusalem 91904, Israel*

ABSTRACT

We present the distribution of the *intrinsic* duration of gamma-ray bursts' prompt emission. This expands upon the analysis of Bromberg et al. (2012) and Bromberg et al. (2013) who showed evidence for collapsar progenitors based on the presence of a plateau in the distribution of T_{90} , the duration over which 90 % of the prompt emission is observed for any given detector. We confirm the presence of this plateau in the distribution of duration corrected for cosmological time dilation (what we call intrinsic duration, T_{int}), but shifted to smaller timescales by a factor of $1/(1+z_{av}) \sim 1/3$, where z_{av} is the average GRB redshift. More significantly, we show this plateau is only present in the sample of GRBs with redshifts greater than $(1+z) \sim 2$, and does *not* appear in the duration distribution of lower redshift GRBs. This result aligns with suggestions that the low redshift population of GRBs has a significant contribution from non-collapsar progenitors (while the high redshift sample is dominated by collapsars). Following Bromberg et al. (2013), we also show the difference in this distribution between spectrally hard and soft GRBs, confirming that a plateau is only present for the soft subset of GRBs. However, when we separate the soft GRBs into low and high redshift subsets, we find that only the high redshift soft GRBs show evidence of a plateau, while the low-redshift soft GRBs do not. This suggests *there exists a significant subset of spectrally soft non-collapsar progenitors at low redshift*. Finally, we use the end time of the plateau to constrain the GRB progenitor density profile and radius, and show the maximum size of a collapsar is a few tenths of a solar radius.

1. INTRODUCTION

Despite many thousands of observations of gamma-ray bursts (GRBs), the most luminous events in our universe, there still remain fundamental questions about the nature of their progenitor systems. We know that many long (duration lasting more than about 2 seconds), spectrally soft GRBs likely result from collapse of massive stars, based on the presence of coincident supernovae in their spectra and light curves (Galama et al. 1998; Hjorth et al. 2003; Woosley & Bloom 2006; Hjorth & Bloom 2012) as well as their locations in star forming regions in their host galaxies (Bloom et al. 2002; Lyman et al. 2017). We have similar circumstantial evidence for short (gamma-ray duration lasting less than about 2 seconds), spectrally hard GRBs associated with compact object mergers, in particular from their locations on the outskirts of their host galaxies, expected from the system's proper motion during the time between formation and merger, first suggested by Narayan et al.

(1992) and later confirmed observationally (e.g. Fong et al. 2010; Fong & Berger 2013). And we have firm evidence that at least one short GRB, GRB170817, is associated with the merger of two neutron stars based on the coincident gravitational waves detected alongside this GRB⁵ (Abbott et al. 2017).

However, the traditional assumption that short, hard GRBs are associated with binary compact object mergers, and that long, soft GRBs result from a massive star collapse has been upended by a number of recent observations and theoretical studies, including evidence of a kilonovae (typically associated with binary neutron stars mergers) in long duration GRBs (Rastinejad et al. 2022; Troja et al. 2022; Yang et al. 2022; Zhang et al. 2022; Yang et al. 2024; Levan et al. 2024, although see Ristić et al. (2025)), a supernova associated with

⁵ We note, however, this may not be a typical short GRB due to its low luminosity, soft spectrum, and unusual time profile (e.g. Kasliwal et al. 2017).

a short GRB (Rossi et al. 2022), and evidence that compact object mergers appear to be the reason behind the uptick in the long GRB rate density at low redshift (Petrosian & Dainotti 2024; Lloyd-Ronning et al. 2024; Chen et al. 2024a). There are also suggestions that certain sub-classes of GRBs potentially originate from distinct progenitors, including low-luminosity GRBs (Soderberg et al. 2006; Guetta & Della Valle 2007), radio bright and radio dark GRBs (Chakraborty et al. 2022; Lloyd-Ronning 2022), short GRBs with extended emission (Metzger et al. 2008; Kaneko et al. 2015), and one GRB that repeated multiple times over a 24 hour period (Levan et al. 2025).

Furthermore, and importantly, some GRBs *appear* as long GRBs, but in fact have very short prompt duration when corrected for cosmological time dilation. Two excellent examples are the very high redshift GRB120923A and GRB090429B. The former, with a measured prompt duration of 27.2 s is at a redshift of $(1+z) = 8.8$ (Tanvir et al. 2018), bringing its intrinsic duration down to just 3 seconds. Meanwhile, GRB090429B is measured at a redshift of $(1+z) = 10.4$ (Cucchiara et al. 2011), bringing its observed duration of 5.8 seconds down to just 0.56 seconds. We discuss these bursts further below, but our point here is that any inferences based on classification by duration need to account for cosmological time dilation.

Recently, machine learning techniques have been developed to help better classify GRBs beyond just the short-hard/long-soft delineation (Luo et al. 2023; Negro et al. 2024; Garcia-Cifuentes et al. 2024; Zhu et al. 2024; Chen et al. 2024b; Espinoza et al. 2025). These techniques often combine highly resolved timing and spectral information into multi-dimensional parameters space, in which “nearest neighbors” are computed to produce a type of map in which similar GRBs tend to cluster. However, using these methods to draw a straightforward connection to the nature of their progenitors is not necessarily clear.

It is likely that many or all of the suggested GRB progenitor systems play a role in producing GRBs, and any distinct signatures of the progenitor are washed out in the cataclysmic event that produces the gamma-ray burst. Nonetheless, efforts toward understanding the relative fraction of possible progenitors systems and how that fraction evolves over cosmic time is not only crucial to understanding GRB physics, but also the evolution of massive stars in general.

An important clue was offered by Bromberg et al. (2012) and Bromberg et al. (2013), who showed that a plateau in the distribution of the observed GRB prompt duration, dN/dT_{90} , provides strong evidence for the presence of a collapsar progenitor⁶. The essential idea is that the observed duration t_γ is the difference between the time over which the central engine is active, t_e , and the minimal activity time of the engine that allows the jet to break out of the stellar envelope, t_{th} , what we call the “threshold time”.⁷ The probability that a GRB has a duration t_γ is equivalent to the probability that the engine has a work time $t_{\text{th}} + t_\gamma$; that is, $p_\gamma(t_\gamma) = p_e(t_{\text{th}} + t_\gamma)$. For observed durations less than a given threshold time, $p_e(t_{\text{th}} + t_\gamma) \approx p_e(t_{\text{th}}) + O(t_\gamma/t_{\text{th}})$ is approximately constant. In other words, $p_\gamma(t_\gamma) \approx p_e(t_{\text{th}}) \approx \text{constant}$, for $t_\gamma < t_{\text{th}}$. Provided the probability distribution of t_e is a relatively smooth function, this necessarily leads to a flat distribution of duration for any engine duration times less than the threshold time of the star (Bromberg et al. 2012, show that this claim holds even for a distribution of threshold times). In other words, under these conditions t_{th} will be the time where the plateau will end in the $p(t)$ distribution.

The probability distribution $p(t)$ is equivalent to dN/dt , the differential number of observed GRBs per unit duration t , not per $\log(t)$ as is normally shown in the literature⁸ (e.g. Kouveliotou et al. 1993). As discussed in Bromberg et al. (2012) and in §4.3 below, this threshold timescale can provide constraints on the progenitor stellar radius and density profile, which – in turn – provide further constraints on the type of stellar system that can produce a GRB.

In this paper, we perform a similar analysis to Bromberg et al. (2012) and Bromberg et al. (2013), but for the so-called *intrinsic duration* distribution, the observed duration corrected for cosmological time dilation. We show that, as expected, this lowers the value of the timescale at which the end (or edge, at the high duration side) of the plateau is evident in the distribution. When analyzing our full sample of about 500 GRBs with measured redshifts, the end of the plateau is around a few seconds (compared to $\gtrsim 10$ seconds seen in the observed T_{90} distribution)

⁶ We note Moharana & Piran (2017) additionally showed evidence for a plateau in the distribution at around 0.4 seconds, interpreted as arising from the jet breaking out the ejecta around a compact binary merger.

⁷ For a non-relativistic jet t_{th} is the actual breakout time from the stellar surface, however in the relativistic case t_{th} is shorter than the breakout time by a factor of $1 - \beta$.

⁸ in which case the plateau becomes a linear increase.

More revealingly, we show that when our sample is divided into “low” and “high” redshift subsets (those with $(1+z) \lesssim 2$ and those with $(1+z) \gtrsim 2$), the plateau only appears in the high redshift sample. The fact that the plateau is not present (or only weakly so) in the low redshift sample supports the conjecture that the population of low redshift GRBs contains a significant fraction of non-collapsar systems, likely compact object mergers, while the sample of high redshift GRBs is composed predominantly of collapsars. When our sample is divided into spectrally “hard” and “soft” subsets, the hardest GRBs do not show evidence of a plateau, while the soft GRBs do; at first glance, this appears to support previous studies claiming spectral hardness is a good indicator of progenitor type. However, when we further divide the spectrally hard and soft samples into low and high redshift subsets, the hard GRB subset does not show evidence of a plateau at either low or high redshifts. The soft sample, on the other hand, shows a clear plateau *only in the high redshift subset*, suggesting the existence of a significant population of spectrally soft non-collapsar progenitors at low redshift. This discovery challenges the traditional classification of collapsars and non-collapsars based on the spectral shape or the hardness ratio (Kouveliotou et al. 1993).

Our paper is organized as follows: In §2, we present our data sample, methods, and discuss potential selection effects and sample completeness. In §3, we present our results: the distribution of the prompt intrinsic (corrected for cosmological time dilation) duration for our whole sample; the distribution of intrinsic duration for GRBs separated into low and high redshift sub-samples; the distribution of intrinsic duration for GRBs separated into spectrally hard and soft GRBs, with the latter also divided into low and high redshift sub-sets. In §4, we present the physical implications of our results. We discuss the ramifications of the presence of a plateau in the higher redshift samples, the lack of a plateau in the lower redshift samples, and how this aligns with studies that have suggested the uptick in the low redshift GRB rate density may be hinting at compact object merger progenitors for these GRBs (regardless of duration and spectral hardness). We also discuss how the end time of the plateau can constrain properties of the progenitor star and provide limits on the collapsar radius, given the average observed properties of the jets in our sample. Finally, in §5, we present our summary and conclusions. Our Appendix provides supplementary data and analysis.

2. DATA AND METHODS

Our data are taken from Wang et al. (2020), who have compiled publicly available observations of 6289 gamma-ray bursts from 1991 to 2016. We searched this dataset for those GRBs with measured redshifts, the vast majority of which are GRBs observed by the *Neil Gehrels Swift Observatory* (492 *Swift* GRBs with redshifts out of the full sample of 567 GRBs with redshift values). We then take the measured T_{90} values (the timescale over which 90% of the prompt emission is observed) and correct it for cosmological time dilation to get the intrinsic duration, T_{int} in the (cosmological) rest frame of the progenitor: $T_{int} = T_{90}/(1+z)$. From this, we construct the duration distribution dN/dT_{int} .

2.1. Selection Effects and Sample Completeness

It is essential to examine the biases present in the data and how they can affect our analysis. There are several issues to consider. Bromberg et al. (2013) showed that the plateau is detector dependent. Indeed, observed duration is detector dependent as instruments not only have different flux sensitivity limits, but their bandpass sensitivities will also affect measured duration. For example, those detectors sensitive to photons over an energy range that aligns with the average peak of the GRB νF_ν distribution (i.e. around a few hundred keV) will tend to have longer T_{90} ’s. We perform our analysis on *only Swift* GRBs to account for this effect.

There is, of course, always a Malmquist-like bias present in any observation (i.e. objects farther away appear fainter). However, the broad GRB luminosity function (the fact that GRBs are not standard candles) largely mitigates this bias. In terms of analyzing the duration distribution of GRBs, where this effect may play the biggest role is through an artificial “shortening” of GRB duration with redshift, also known as the “tip-of-the-iceberg” effect. This effect on the sample of long GRBs was discussed in Nakar & Piran (2002); Piran (2004) as well as Lloyd-Ronning et al. (2023) who corrected for this bias using non-parametric methods of Lynden-Bell (1971) and Efron & Petrosian (1992). They showed that, again, because GRBs are not standard candles this effect is weakened and its influence on the behavior of the overall duration distribution is relatively small (although see the analysis of Moss et al. 2022).

A potentially more important selection effect is one against detecting short GRBs at high redshifts. The issue here is not so much a problem of short GRBs having lower prompt gamma-ray luminosity (and therefore be-

Table 1. Parameters from equation 1, fit to the different dN/dT distributions. We do not list the values of β in the table below as all the fits returned $\beta = 0$. Note for the low redshift and hard sub-samples, the value of T_B is relatively low but has an error bar many times greater than the fit value, indicating there is no clear plateau in these data.

Dataset	A_{NC}	μ	σ	A_C	α	T_B (s)	χ^2/dof
T_{90}	-28.9 ± 13.5	2.3 ± 1.5	-4.3 ± 2.7	3.1 ± 1.0	-0.4 ± 0.1	8.2 ± 5.1	1.01
T_{int}	3.1 ± 3.1	-0.5 ± 9.3	6.2 ± 10.9	1.0 ± 0.3	-0.5 ± 0.1	2.5 ± 1.1	0.87
T_{int} , Low z	5.7 ± 3.0	1.4 ± 0.8	2.9 ± 0.8	0.1 ± 0.4	-0.3 ± 0.5	4.1 ± 19.2	0.33
T_{int} , High z	50.3 ± 19.2	2.4 ± 0.3	1.8 ± 0.3	1.3 ± 0.8	-0.5 ± 1.1	15.8 ± 6.6	0.67
T_{int} , Hard	-156.0 ± 33969.8	-13.0 ± 4318.2	-29.7 ± 5644.2	-0.1 ± 0.7	-1.0 ± 23.5	8.0 ± 126.6	0.97
T_{int} , Soft	92.1 ± 42.5	2.1 ± 0.5	1.8 ± 0.3	2.4 ± 1.5	-0.6 ± 0.9	18.0 ± 9.7	0.56
T_{int} , Soft, Low z	42.3 ± 68.0	1.6 ± 2.7	2.6 ± 2.2	1.5 ± 5.9	-0.3 ± 1.1	2.4 ± 11.5	1.70
T_{int} , Soft, High z	5.3 ± 2.9	1.3 ± 0.1	0.3 ± 0.2	1.3 ± 0.3	-0.3 ± 0.7	13.7 ± 8.0	0.82

ing harder to trigger on or detect at high redshift). In fact, several studies have shown short GRBs luminosities are comparable to long GRBs, especially in terms of the break in the luminosity function (Wanderman & Piran 2015; Ghirlanda et al. 2015; D’Avanzo 2015; Ghirlanda et al. 2016), although see Wanderman & Piran (2015); Dainotti et al. (2021), who show that the short GRB luminosity function falls more steeply above the break than that of long GRBs, which can cause a bias against detecting high redshift short GRBs.

However, perhaps the more important problem lies in their lack of afterglow detection. Many short GRBs are found in the outskirts of their host galaxies (Fong et al. 2010; Fong & Berger 2013; Castrejon et al. 2025), in environments of lower circumburst density. Additionally, short GRBs have on average smaller isotropic-equivalent energies E_{iso} than long GRBs. Both of these factors make their afterglows harder to detect and therefore a redshift determination untenable. Because we are examining only the sample of GRBs with redshift measurements, this bias may certainly affect our sample. Interestingly, for the few short GRBs with opening angle measurements, the beaming corrected energy is not much smaller than that of long GRBs; furthermore, there are quite a few short GRBs at large offsets from their host galaxies that still show observable afterglow emission (Fong & Berger 2013). Therefore, the extent of an observational bias against detecting high redshift short GRBs is not entirely clear. We revisit this issue – and how it can affect the interpretation of our results – further below in §4.

Finally, we also separate our sample by hardness classes, as in Bromberg et al. (2013). Definitions of spectral hardness vary depending on the instrument detecting the GRB (and its detector response as a function of energy). Because our sample is comprised of GRBs

detected by *Swift*, which is sensitive to relatively low gamma-ray energies compared to other GRB detectors, we use the “steepness” of the photon spectral index according to either a single power-law or cutoff power-law fit (discussed in more detail in the next section). However, it should be noted that spectral hardness can be inherently difficult to characterize. For example, because *Swift* is only sensitive to energies of up to 200 keV, whereas the peak energy of a GRB spectrum often falls in the range of several hundreds of keV, there may exist GRBs with a relatively soft low energy photon index, but a very high peak energy or shallow high energy photon index which would indicate the burst is much harder than it appears in the *Swift* bandpass.

With these potential biases in mind, we proceed with our analysis of the dN/dT distribution (and discuss further below where they may play a role in shaping our results), again focusing on the sample of *Swift* GRBs with redshifts.

2.2. Quantifying the Timescale of the Plateau

To quantify the time when the plateau ends we fit the duration distribution of our samples with a combination of two analytic functions for the distribution of Collapsars and non-Collapsars, taken from Bromberg et al. (2013, Eq. 1) and shown below. The non-collapsar (NC) component modeled by a log-normal distribution, while the collapsar (C) component is modeled by a constant below some characteristic time $T_{int} \leq T_B$ and a power-law plus exponential cutoff above this time $T_{int} > T_B$:

$$\frac{dN}{dT_{int}} = A_{NC} \frac{1}{T_{int} \sigma \sqrt{2\pi}} e^{-\frac{(\ln T_{int} - \mu)^2}{2\sigma^2}} + A_C \begin{cases} 1 & T_{int} \leq T_B \\ \left(\frac{T_{int}}{T_B}\right)^\alpha e^{-\beta(T_{int} - T_B)} & T_{int} > T_B \end{cases} \quad (1)$$

When the fit is reasonable (in the sense of each component of the function is a good description of the total data), then T_B roughly represents the time of end time of the plateau.

3. RESULTS

Figures 1 - 4 show our dN/dT_{int} distributions, and Table 1 shows the best fits to these distributions according to equation 1.

Figure 1 shows the distribution of the intrinsic duration, dN/dT_{int} (magenta), as well as observed duration, dN/dT_{90} (green), for the *Swift* GRBs with measured redshifts, binned into equally spaced bins. The magenta and green histograms are artificially offset by one order of magnitude along the y-axis, for clarity of comparison, and we assume Poisson statistics to estimate the errors in each bin. The end of the plateau in the T_{int} distribution appears at shorter durations than that of T_{90} , occurring around just a few seconds (compared to ~ 10 's of seconds in the T_{90} duration). The ratio between where the plateau ends occur (according to our fits shown in Table 1 and as evident by eye) is a factor of $\sim 1/3$, consistent with the correction due to cosmological time dilation for the average redshift of a GRB, $1/(1+z_{av})$. We note that our T_{90} distribution – specifically where the end of the plateau occurs – for those *Swift* GRBs with redshift measurements agrees with that of Bromberg et al. (2012), who show the T_{90} distribution for all *Swift* GRBs both with and without redshift (see their Figure 1).

3.1. Redshift Separated Distributions

Figure 2 shows the intrinsic duration distribution, dN/dT_{int} , for all of our *Swift* GRBs, divided into “lower” redshift (blue lines) and “higher” redshift (orange lines) sub-samples, with a delimiting value of $(1+z) = 2.2$. The high redshift sample shows a clear plateau from ~ 0.1 s up to around ~ 15 s (confirmed by our fits shown in Table 1), with no evidence of any uptick or “non-collapsar” increase at low durations. In contrast, and again confirmed by our fits using the function in equation 1, the low redshift distribution shows no evidence of a plateau.

The distinction in the dN/dT_{int} distributions between low and high redshift GRBs appears to show up most prominently when using a delimiting value of redshift between $(1+z) = 2$ to 2.5 (in the Appendix we show how this plot changes as a function of the redshift delimiter), suggesting that non-collapsar progenitors begin to play a more dominant role in producing GRBs below this redshift, while above this redshift, collapsars will

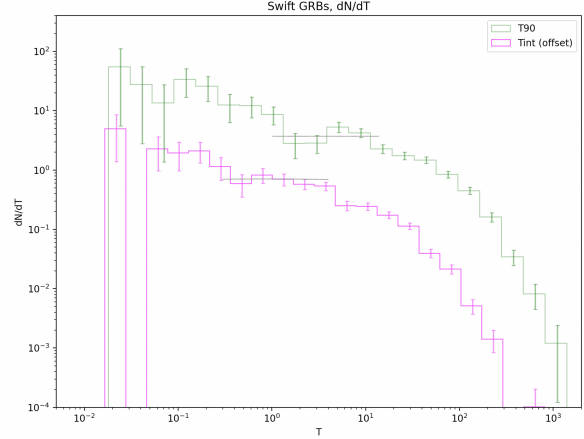


Figure 1. dN/dT distribution of both T_{90} (green line) and intrinsic duration T_{int} (magenta line), for our sample of *Swift* GRBs with redshifts; the distributions are artificially offset by a constant along the y-axis for comparison purposes. The right edge of the lines indicates the end of the plateau. The end of the plateau of the intrinsic duration distribution is shifted to shorter timescales by a factor of $\sim 1/3$. Table 1 gives the best-fit parameters of these distributions according to equation 1.

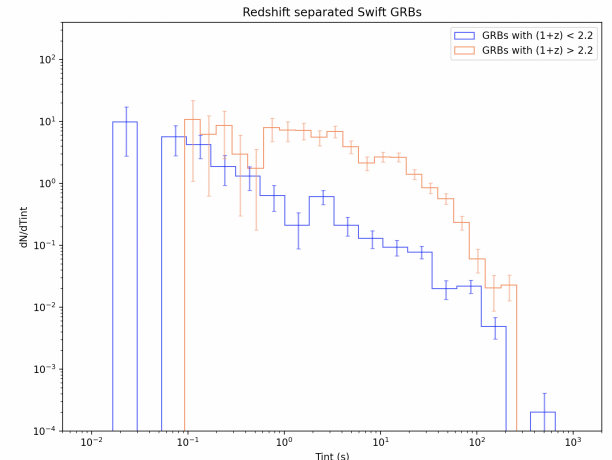


Figure 2. dN/dT distribution of intrinsic duration, T_{int} , broken into “low” redshift (blue lines) and “high” redshift (orange lines), with a redshift delimiter of $(1+z) = 2.2$. There is a clear plateau in the high redshift sample, while no plateau present in the low redshift sample. The fits to these distributions, according to equation 1, are given in Table 1.

dominate the progenitors of GRBs.

The lack of short GRBs in the high redshift sample may be attributed to the observational biases discussed in §2. Nevertheless, there are strong physical reasons to expect a real deficit of high redshift short GRBs,

due to long delay times between progenitor formation and compact-object merger, which result in a shift of a large fraction of these events to low redshift (on the order of a Hubble time for most of them; Piran 1992; Guetta & Piran 2006; Nakar et al. 2006; Berger et al. 2007; Lee 2010; Coward et al. 2012; Hao & Yuan 2013; Wanderman & Piran 2015; Anand et al. 2018; Belczynski et al. 2018; Chruslinska et al. 2018; Broekgaarden et al. 2022; Santoliquido et al. 2022; Zevin et al. 2022; Maoz & Nakar 2024). This means that most of the short GRBs (if the majority of this population comes from compact object mergers) are expected to occur at lower redshifts, and that this is not simply due to an observational selection effect.

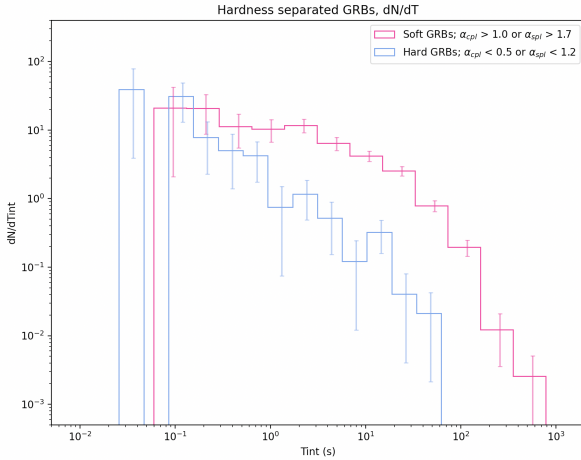


Figure 3. dN/dT distribution of intrinsic duration, T_{int} , for *Swift* GRBs with redshift, broken into “hard” and “soft” sub-samples based on the power-law index and spectral fit model. A plateau is present in the soft sample with an end at around a few seconds, while there is no plateau in the hard sample, confirming the results of Bromberg et al. (2013). The fits to these distributions, according to equation 1, are given in Table 1.

3.2. Hardness Separated Distributions

Bromberg et al. (2013) was one of the first studies to suggest that there is a non-negligible fraction of long duration ($\gtrsim 10$ s) non-collapsar GRBs. They showed this by separating GRBs according to their spectral hardness and demonstrating that the plateau (the telltale collapsar signature) is not present in the hardest subset of GRBs, regardless of duration, while it is present in the softest subset of GRBs. Hence, they suggest that spectral hardness might be a better indicator of progenitor class, compared to duration. We perform a similar analysis here, for the spectrally separated duration distribu-

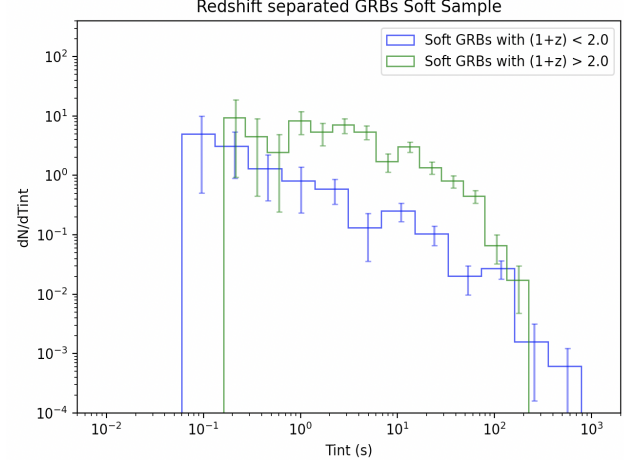


Figure 4. dN/dT distribution of intrinsic duration, T_{int} , for the *Swift* GRB spectrally soft sample broken into “low” redshift (blue lines) and “high” redshift (green lines), with a redshift delimiter of $(1 + z) = 2.0$. Even within the soft sample we see a lack of a plateau in the low redshift GRBs, and a clear plateau in the high redshift GRBs, confirmed by our fits to equation 1, shown in Table 1.

tion corrected for cosmological time dilation. Because definitions of spectral hardness are detector dependent, we emphasize again that we are only analyzing the *Swift* GRBs in our sample. We have divided our bursts into hardness classes according to the steepness of its low energy spectral photon index, for two different models of the spectrum. The first is a single power-law (*spl*):

$$N(E) = A_{spl} E^{-\alpha_{spl}} \quad (2)$$

and the second is a power-law with an exponential cutoff (*cpl*):

$$N(E) = A_{cpl} E^{-\alpha_{cpl}} \exp^{-E/E_c} \quad (3)$$

where A is a normalization factor, and E_c is the cutoff energy. Each model has a different criterion for what constitutes spectral hardness. In the Appendix, we show the spectral indices of as a function of T_{90} for all GRBs for which these fits are available, and show where we have chosen to draw our cuts for what constitutes “hard” and “soft” for each model, where “hard” is defined as a value of α above the upper cutoff line and “soft” is defined as a value of α below the lower cutoff line.

Figure 3 shows our hard (light blue) and soft (pink) *Swift* GRBs. Consistent with Bromberg et al. (2013), but – again – shown here for the intrinsic duration distribution, we see that the hardest GRBs show no evidence of a plateau, while soft GRBs show evidence of a plateau end at around a few seconds. Figure 4 shows the

dN/dT_{int} distribution of our soft sample, but divided into low and high redshift groups. As with the entire sample, we see that the lower redshift group does not show evidence of a plateau, confirmed by our fits shown in Table 1. This means that there exists a significant population of spectrally soft non-collapsar progenitors at low redshift. We note that when the spectrally hard GRBs are split into low and high redshift sub-samples, there is no evidence of a plateau in either distribution (at low or high redshift), suggesting spectrally hard GRBs are indeed dominated by non-collapsars across cosmic time. However, the number of GRBs in this sample is too small to put this statement on firm statistical footing.

3.3. Summary of Results

For the intrinsic duration distribution of our whole sample of *Swift* GRBs with redshift, the end of the plateau is (unsurprisingly) shifted to lower timescales by a factor of $\sim 1/(1+z_{av})$, where z_{av} is the average redshift of the GRB population. For the redshift separated distributions, the end time of the plateau in the *high redshift* sample appears at around ~ 10 to 15 seconds, while there is no plateau apparent in the low redshift sample. For the hardness-separated sub-samples, the plateau occurs at about 10 seconds in the soft sample, while there is no apparent plateau in the spectrally hard sample. Finally, for the redshift-separated spectrally soft sample, the plateau remains in the high redshift sample (with an end time at around ~ 10 s), but there is no apparent plateau in the spectrally soft, low redshift sample. All of these statements are quantified in Table 1 for the different sample subsets. We note that the fitting results do depend on the binning of the data and occasionally the function does not always characterize the data well. For example, for the low redshift and hard sub-samples, the error bars on T_B are many times greater than the value of T_B itself. This indicates that there is no firm T_B value for these data – in other words, there is no plateau in these distributions.

The primary takeaway from this analysis is that GRBs at redshifts $(1+z) \gtrsim 2$ are dominated by collapsar progenitors, while the GRB sample at redshifts $(1+z) \lesssim 2$ appear to be dominated by non-collapsar progenitors, regardless of spectral hardness.

4. PHYSICAL IMPLICATIONS

The fact that the plateau is evident in some of our sub-samples and not in others, combined with the plateau end time values when it *is* present has a number of implications. First, we note the disparity in the plateau end

times between the different T_{int} distributions (i.e. Figures 1 - 3), when the plateau is clearly present. This is likely a result of an imperfect fit of our analytic functions to the GRB duration distribution. When the number of non-collapsars increases, it pushes A_C to higher values (i.e. raises the height of the fitted plateau); as a result, the best-fit value of T_B is reduced. In other words, the fit of T_B better captures the true end time of the plateau in samples that are less contaminated by non-collapsars, such as the sample of high redshift GRBs (those GRBs with $(1+z) \gtrsim 2$). It is this timescale of ~ 10 seconds that is probably the best characterization of the collapsar threshold time, the minimum engine working time that will allow the jet to exit the star. As such, when we use the plateau end timescale to constrain progenitor properties below, we use the average properties of the jet (the jet luminosity and opening angle) from this particular high redshift sub-sample.

4.1. On the Plateau in the Redshift Separated Sub-samples

A number of studies have shown there is an uptick in the low redshift rate density distribution of GRBs, even when carefully and conservatively accounting for selection effects in the data (Petrosian et al. 2015; Yu et al. 2015; Tsvetkova et al. 2017; Le & Mehta 2017; Lloyd-Ronning et al. 2019; Le et al. 2020; Lloyd-Ronning et al. 2020; Hasan & Azzam 2024; Khatiya et al. 2025)⁹. Several groups have provided models and arguments for this uptick (e.g. Petrosian & Dainotti 2024; Lloyd-Ronning et al. 2024). In particular they have shown that compact object merger progenitors (e.g. double neutron star mergers and white dwarf-black hole mergers) naturally produce this uptick at low redshifts because of their delay time distributions from formation to merger. In other words, the time from the binary formation to the merger event (when the GRB occurs) is on the order of the Hubble time and therefore there is an accumulation of these events at low redshift (relative to their rates at high redshift). We note the analysis of the uptick in the rate density at low redshifts focused on long-duration GRBs, so this assumes these progenitor systems can produce a long GRB (which appears to be a reasonable assumption, e.g., Fryer et al. 1999; Zhu et al. 2022; Gottlieb et al. 2023; Lloyd-Ronning et al. 2024; Chrimes et al. 2025).

⁹ Although see Perley et al. (2016) who note that when a redshift-dependent efficiency of GRB formation from a given progenitor is included in the analysis, this uptick can go away. Additionally, Lloyd-Ronning et al. (2020) showed that when accounting for jet opening angle evolution with redshift, the uptick is reduced (although still present).

Meanwhile, the clear presence of a plateau in the higher redshift sample aligns with the expectation that collapsar progenitors of GRBs favor lower metallicity environments (MacFadyen & Woosley 1999; Yoon & Langer 2005; Hirschi et al. 2005; Yoon et al. 2006; Woosley & Heger 2006). In other words, if collapsars are indeed more likely to form in low metallicity environments (as suggested by the studies cited above), then it is natural to expect them to occur more readily at higher redshifts where the average metallicity of the universe is lower.

4.2. On the Plateau in the Spectrally Separated Sub-samples

Similar to what was shown in Bromberg et al. (2013) for the T_{90} distribution, there is no apparent plateau in the T_{int} distribution for our spectrally hard subset of GRBs, shown in Figure 3, suggesting these GRBs are dominated by non-collapsar progenitors. We might then expect that the hard bursts have on average lower redshifts, aligning with the results mentioned in the previous section that low redshift bursts appear to be dominated by non-collapsar progenitors.

However, interestingly, the average redshift of both the soft and the hard samples is ~ 3 . A very big caveat is that our hard sub-sample is relatively small, with only about 25 GRBs. Within this small sample, there are two GRBs at extremely high redshift (mentioned in the Introduction): GRB120923A at a redshift of $(1+z) = 8.8$ and GRB090429B with $(1+z) = 10.3$. When those “outliers” are removed and we look at only GRBs with $(1+z) < 6$, we find the average redshift of the soft sample is $(1+z) = 2.9$ and the hard sample is $(1+z) = 2.2$. A Student’s t-test shows a marginal difference ($\sim 2\sigma$) between the averages of these two distributions, although again we caution that the numbers in the hard sample are small and so any statistical analysis comparing these distributions is not on firm footing. Nonetheless, it seems clear that there is not a simple correspondence between hard bursts (seemingly dominated by non-collapsar progenitors) and low redshift bursts (also seemingly dominated by non-collapsar progenitors). Indeed this aligns with our analysis in Figure 4 indicating the existence of a class of spectrally soft low-redshift GRBs.

We note that Beniamini & Piran (2019) and Maoz & Nakar (2025) have presented compelling evidence for a population of “fast” mergers, binary neutron star systems that merge in less than 1 Gyr, which would produce a subset of non-collapsar GRBs at *high* redshift. This could explain the two very high redshift GRBs mentioned above, which are both spectrally hard

and short in their intrinsic duration, and the fact that hard GRBs do not show evidence of a plateau in their dN/dT_{int} distribution, regardless of redshift. We defer a detailed analysis of these GRBs to a future paper.

4.3. Can We Constrain the Properties of Collapsar Progenitors?

The end of the plateau in the duration distribution is related to what we defined as the “threshold time”, t_{th} , in §1. This is the minimum central engine working time necessary in order for the jet to break out of the star, assuming that the central engine stops abruptly and that the information about the shutoff propagates to the jet head at the speed of light:

$$t_{th} = t_R - R/c, \quad (4)$$

where R is the stellar radius (including the envelope) and

$$t_R = \int_0^R \frac{dr}{\beta_h(r)c} \quad (5)$$

is the time it takes the jet head to reach the edge of the star. Another way to think about this timescale is as follows: imagine a jet propagating through the star, and at some point the central engine shuts off abruptly. The shutoff time for which the information about the loss of power catches up with the jet head at the edge of the star is this threshold time. This is the timescale at which we expect the end of the plateau end to appear in the duration distribution of collapsar jets.

We now consider this threshold time for different progenitor models, characterized by their density profiles and stellar radii. To calculate the threshold time for a given stellar model we need to compute the ratio of the jet energy density to that of the surrounding medium (the rest-mass energy density) at the location of the jet head, defined as \tilde{L} (Matzner 2003; Bromberg et al. 2011):

$$\tilde{L} = \frac{\rho_j(1 + 4P_j/\rho_j c^2)\Gamma_j^2}{\rho_*}, \quad (6)$$

where we assume here a hydrodynamic jet. This ratio sets the velocity of the jet head and, in particular, whether the jet head is relativistic or not. Values of $\tilde{L} \ll (\gg) 1$ correspond to a non-relativistic (relativistic) head velocity. To determine this quantity, and therefore measure the jet head speed to be used in equations 4 and 5, we do the following:

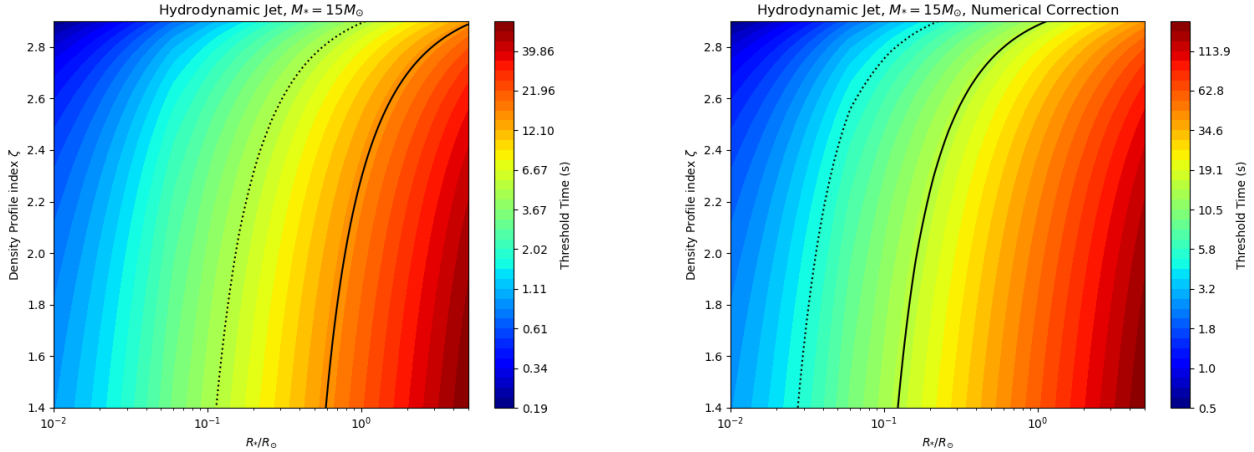


Figure 5. Threshold time as a function of stellar radius (x-axis) and the stellar density profile index (y-axis) for a star of 15 solar masses. The black dotted and solid lines mark a timescale of 5 seconds and 15 seconds, respectively (corresponding to the range of plateau end times in our dN/dT_{int} distributions). The left panel shows the threshold time scale based on equation 4, while the right panel applies a correction to this equation based on the numerical simulations of Harrison et al. (2018). We used the average (beaming-corrected) jet luminosity and opening angle of our high redshift sample in these calculations.

- For each stellar profile, we calculate $\tilde{L}(r)$, using equation 3 from Bromberg et al. (2011):

$$\tilde{L} = \frac{L_j}{\rho_*(r)c^3\Sigma_j(r)}, \quad (7)$$

where $\rho_*(r)$ is the stellar density at radius r and $\Sigma_j(r)$ is the jet cross section radius when the jet head is at point r . To calculate Σ_j , we assume that the jet is collimated, $\Sigma_j \simeq \frac{L_j\theta_o^2}{4cp_c}$ (their equation 12), where L_j is the jet luminosity, θ_o is the half-opening angle of the jet, and p_c is the cocoon pressure.

- We assume a power-law density profile for our progenitor star over the region the jet propagates, $\rho_*(r) = \rho_o(r/r_o)^{-\zeta}$. Realistic stellar density profiles do not necessarily follow a single power-law structure but stellar structure simulations of GRB progenitors have shown this can be a good approximation over our region of interest (e.g. Woosley & Heger 2006; Aguilera-Dena et al. 2020; Halevi et al. 2023). Although the average power-law index can vary substantially across models, it is generally confined between values of $\sim 1.5 - 2.5$.
- We calculate two functions of $\tilde{L}(r)$ using the non-relativistic, and relativistic expressions for the cocoon pressure p_c , given in the Appendix of Bromberg et al. (2011). This results in $\tilde{L}_{NR} \propto (\rho_*r^2)^{-2/3}$ (typical for the inner part of the star) and $\tilde{L}_R \propto (\rho_*r^2)^{-2/5}$ (typically at the outer parts of the star) for the non-relativistic (NR) and relativistic (R) expressions, respectively. We locate

the radius where $\tilde{L}_{NR}(r_*) = \tilde{L}_R(r_*)$. At $r < r_*$ we use the non-relativistic expression, and at $r > r_*$ we used the relativistic expression.

- Finally, we obtain the jet head 3-velocity using:

$$\beta_h(r) \simeq \frac{1}{1 + \tilde{L}^{-1/2}}. \quad (8)$$

and integrate it using equation 5 to obtain the breakout time of the jet head from the star and substitute the result in equation 4 to obtain the threshold time.

Our results are shown in Figure 5, which displays contour plots of the threshold time for different values of the density power-law index and stellar radius, assuming a progenitor mass of $15M_\odot$. We have set θ_o equal to the average value of the jet opening angle in our high redshift sample ($\theta_o = \theta_j \approx 5.8^\circ$), and set the jet luminosity equal to the average value of the (beaming corrected) jet luminosity in our high redshift sample, $L_j \approx 1.9 \times 10^{50} \text{ erg/s}$.¹⁰ We show similar contour plots over a wider range of parameter space (e.g. different luminosities, progenitor masses, and jet opening angles) in the Appendix. The black dotted and solid lines mark thresholds times of 5 seconds and 15 seconds, respectively. This corresponds to the range of

¹⁰ Note in our soft sample, the average opening angle is $\theta_j = 6.3^\circ$, while the average (beaming corrected) jet luminosity is $L_j = 0.7 \times 10^{50} \text{ erg/s}$.

plateau end times in the dN/dT distributions we find in our collapsar-dominated data samples above. Again, we argue that the higher redshift sample (orange line in Figure 2) is the subset least contaminated by non-collapsar progenitors, and has an plateau end time of about 10 to 15 seconds.

The left plot shows the threshold time under the idealized assumptions described above, calculated in equation 4. We can see for threshold times less than about 15 seconds, GRB collapsar progenitors are constrained to radii less than a solar radius for density profiles shallower than $\zeta \lesssim 2.5$. The right plot shows the same threshold time, but with a numerical correction applied to the equation, as described in Harrison et al. (2018). This study found, performing hydrodynamic simulations of a jet propagating through a star with a given density profile, that the simulated threshold time is larger by a factor of ~ 2 to 3 compared to the purely analytic estimate.¹¹ In this case, progenitor radii are constrained to very small values less than a few tenths of a solar radius.

We note that Gottlieb et al. (2022) point out that density profiles that are too steep (with $\zeta > 2$) require over-luminous jets (relative to observed luminosities) to overcome the central high density of the progenitor. They suggest that only progenitors with $\zeta \leq 2$ will produce GRB jets consistent with observations, under the assumption of a threshold time around 10 seconds and provided the radiative efficiency is relatively high.¹²

Our analysis above is done for a hydrodynamic jet. This assumption is consistent with the results of (Gottlieb et al. 2020, 2021, 2022) who show significant magnetic energy dissipation in collapsar jets reducing the jet magnetization σ to values $\lesssim 0.1$ deep in the stellar core. We point out that magnetic jets are subject to various types of instabilities like the kink instability, which can render them unstable especially in media with a flat density distribution ($\zeta \leq 2$) (Bromberg & Tchekhovskoy 2016), resulting in longer breakout times.

¹¹ The physical reason behind this is that the jet has a wider effective cross section in the simulations compared to the simple analytic estimate, causing the propagation speed to slow down by a factor of ~ 2 to 3. See Harrison et al. (2018) for further details.

¹² If, instead, one assumes that only a small fraction of jet power is going into the observed radiation, the jet luminosity is much higher than what is inferred from the prompt emission and there is no such a stringent constraint on density index. If this were the case, our jet luminosities would be much higher than the values we are using above and the radius of the progenitor would be constrained to be even smaller.

Finally, we point out that the value of the threshold time we infer from the intrinsic duration distribution is consistent with the detailed numerical simulations of Urutia et al. (2025), of magnetically launched jets propagating through the Wolf-Rayet stellar models of Woosley & Heger (2006).

5. SUMMARY AND CONCLUSIONS

We have re-analyzed the duration distribution of GRBs, following the methods of Bromberg et al. (2012, 2013), but using the *intrinsic* prompt duration, corrected for cosmological time dilation. Additionally, we have split our sample into “low” and “high” redshift, as well as spectrally “hard” and “soft”, sub-samples and found that the distributions differ significantly between these sub-samples. This has important implications for the types of GRBs that dominate at different epochs in the history of our universe. Our main results are as follows:

- We show the presence of a plateau in the *intrinsic* duration distribution, dN/dT_{int} , where T_{int} is the observed duration corrected for cosmological time dilation, for *Swift* GRBs with measured redshifts. We find the plateau end is shifted to lower durations by a factor of $1/(1+z_{av})$, where z_{av} is the average GRB redshift. It occurs at around a few seconds, and not 10’s of seconds as seen in the *observed* prompt duration distribution (T_{90}).
- When we break the sample into lower and higher redshift sub-sets, with a delineating redshift of $(1+z) \sim 2$, we find the strong presence of a plateau in the high redshift sample, with an end at around 10 to 15 seconds and no evidence of a plateau in the low redshift sample of GRBs. We suggest this aligns with recent studies that have claimed that the low redshift sample is dominated by non-collapsar (potentially compact object merger) progenitors.
- When our sample is split into spectrally harder and softer sub-samples, the spectrally hard sample exhibits no plateau in the distribution, while the spectrally soft sample exhibits a clear plateau. This confirms what was found in Bromberg et al. (2013) for the T_{90} distribution. Furthermore, although spectrally hard GRBs appear to be dominated by non-collapsars across redshifts, spectrally soft GRBs show a dichotomy between low and high redshift sub-samples. When the spectrally soft sample is separated into low and high redshift groups, the plateau only appears in the high redshift sample while there is no plateau in the spec-

trally soft low-redshift sample, shown in Figure 4. This suggests *there exists a significant population of spectrally soft non-collapsar progenitors at low redshift*.

- Connecting the end time of the plateau to the “threshold time” (the minimum central engine required to push the jet out of the star) of a typical hydrodynamic collapsar jet, we use our results to constrain the radius of the progenitor star. We show that, when realistic assumptions about the jet head cross section and propagation velocity are accounted for, it must be less than only a few *tenths* of a solar radius. Although it has long been argued that GRBs should come from stripped envelope stars, these envelopes can in some cases be optically thick and this analysis puts relatively strong limits on the extent and density of the wind envelope around GRB progenitors.

As we continue to discover interesting examples of GRBs that upend our traditional picture of classifying their progenitors according to whether the observed prompt gamma-ray burst is long/soft or short/hard, looking for other signatures in the data that may help clarify the progenitor paradigm is more important than ever. Telescopes like the *Einstein Probe* have, for example, discovered X-ray transients at rates consistent with GRB event rates and redshift distributions (O’Connor

et al. 2025; Gao et al. 2025). *SVOM* has begun detecting short duration GRBs out to high redshifts (Dimple et al. 2025). Meanwhile, an emerging multi-messenger astrophysics community is coordinating efforts to optimize the follow-up of GRBs across detector capabilities. With the advent of these new observatories and observing strategies, we are poised to access the keys to unlocking the mystery behind these most extreme events in our universe.

ACKNOWLEDGMENTS

This work was supported by the U. S. Department of Energy through Los Alamos National Laboratory (LANL). LANL is operated by Triad National Security, LLC, for the National Nuclear Security Administration of U.S. Department of Energy (Contract No. 89233218CNA000001), LA-UR-25-31112. O.B. was supported by an ISF grant 2067/22, a BSF grant 2024297 and NSF-BSF grants 2020747 & 2024788. T.P. acknowledges support from an Advanced ERC grant MultiJets, ISF grant 2126 and the Simon foundation SCEECS collaboration.

AUTHOR CONTRIBUTIONS

All authors contributed equally to the collaboration.

REFERENCES

Abbott, B. P., Abbott, R., Abbott, T. D., et al. 2017, Physical Review Letters, 119, 161101, doi: [10.1103/PhysRevLett.119.161101](https://doi.org/10.1103/PhysRevLett.119.161101)

Aguilera-Dena, D. R., Langer, N., Antoniadis, J., & Müller, B. 2020, ApJ, 901, 114, doi: [10.3847/1538-4357/abb138](https://doi.org/10.3847/1538-4357/abb138)

Anand, N., Shahid, M., & Resmi, L. 2018, MNRAS, 481, 4332, doi: [10.1093/mnras/sty2530](https://doi.org/10.1093/mnras/sty2530)

Belczynski, K., Bulik, T., Olejak, A., et al. 2018, arXiv e-prints, arXiv:1812.10065, doi: [10.48550/arXiv.1812.10065](https://doi.org/10.48550/arXiv.1812.10065)

Beniamini, P., & Piran, T. 2019, MNRAS, 487, 4847, doi: [10.1093/mnras/stz1589](https://doi.org/10.1093/mnras/stz1589)

Berger, E., Fox, D. B., Price, P. A., et al. 2007, ApJ, 664, 1000, doi: [10.1086/518762](https://doi.org/10.1086/518762)

Bloom, J. S., Kulkarni, S. R., & Djorgovski, S. G. 2002, AJ, 123, 1111, doi: [10.1086/338893](https://doi.org/10.1086/338893)

Broekgaarden, F. S., Berger, E., Stevenson, S., et al. 2022, MNRAS, 516, 5737, doi: [10.1093/mnras/stac1677](https://doi.org/10.1093/mnras/stac1677)

Bromberg, O., Nakar, E., Piran, T., & Sari, R. 2011, ApJ, 740, 100, doi: [10.1088/0004-637X/740/2/100](https://doi.org/10.1088/0004-637X/740/2/100)

—. 2012, ApJ, 749, 110, doi: [10.1088/0004-637X/749/2/110](https://doi.org/10.1088/0004-637X/749/2/110)

—. 2013, ApJ, 764, 179, doi: [10.1088/0004-637X/764/2/179](https://doi.org/10.1088/0004-637X/764/2/179)

Bromberg, O., & Tchekhovskoy, A. 2016, MNRAS, 456, 1739, doi: [10.1093/mnras/stv2591](https://doi.org/10.1093/mnras/stv2591)

Castrejon, C., Nugent, A. E., Fong, W.-f., et al. 2025, arXiv e-prints, arXiv:2508.20156, doi: [10.48550/arXiv.2508.20156](https://doi.org/10.48550/arXiv.2508.20156)

Chakraborty, A., Dainotti, M., Cantrell, O., & Lloyd-Ronning, N. 2022, Radio-bright vs. Radio-dark Gamma-ray Bursts - More Evidence for Distinct Progenitors, arXiv:2210.12972 [astro-ph.HE]. <https://arxiv.org/abs/2210.12972>

Chen, J., Shen, R.-F., Tan, W.-J., et al. 2024a, arXiv e-prints, arXiv:2409.00472. <https://arxiv.org/abs/2409.00472>

Chen, J.-M., Zhu, K.-R., Peng, Z.-Y., & Zhang, L. 2024b, MNRAS, 527, 4272, doi: [10.1093/mnras/stad3407](https://doi.org/10.1093/mnras/stad3407)

Chrimes, A. A., Gaspari, N., Levan, A. J., et al. 2025, arXiv e-prints, arXiv:2508.10984, doi: [10.48550/arXiv.2508.10984](https://doi.org/10.48550/arXiv.2508.10984)

Chruslinska, M., Belczynski, K., Klencki, J., & Benacquista, M. 2018, MNRAS, 474, 2937, doi: [10.1093/mnras/stx2923](https://doi.org/10.1093/mnras/stx2923)

Coward, D. M., Howell, E. J., Piran, T., et al. 2012, MNRAS, 425, 2668, doi: [10.1111/j.1365-2966.2012.21604.x](https://doi.org/10.1111/j.1365-2966.2012.21604.x)

Cucchiara, A., Levan, A. J., Fox, D. B., et al. 2011, ApJ, 736, 7, doi: [10.1088/0004-637X/736/1/7](https://doi.org/10.1088/0004-637X/736/1/7)

Dainotti, M. G., Petrosian, V., & Bowden, L. 2021, ApJL, 914, L40, doi: [10.3847/2041-8213/abf5e4](https://doi.org/10.3847/2041-8213/abf5e4)

D'Avanzo, P. 2015, Journal of High Energy Astrophysics, 7, 73, doi: [10.1016/j.jheap.2015.07.002](https://doi.org/10.1016/j.jheap.2015.07.002)

Dimple, Gompertz, B. P., Levan, A. J., et al. 2025, MNRAS, 544, 548, doi: [10.1093/mnras/staf1574](https://doi.org/10.1093/mnras/staf1574)

Efron, B., & Petrosian, V. 1992, ApJ, 399, 345, doi: [10.1086/171931](https://doi.org/10.1086/171931)

Espinoza, S. N., Lloyd-Ronning, N. M., Negro, M., Cheng, R. M., & Cibrario, N. 2025, Research Notes of the American Astronomical Society, 9, 239, doi: [10.3847/2515-5172/ae031c](https://doi.org/10.3847/2515-5172/ae031c)

Fong, W., & Berger, E. 2013, ApJ, 776, 18, doi: [10.1088/0004-637X/776/1/18](https://doi.org/10.1088/0004-637X/776/1/18)

Fong, W., Berger, E., & Fox, D. B. 2010, ApJ, 708, 9, doi: [10.1088/0004-637X/708/1/9](https://doi.org/10.1088/0004-637X/708/1/9)

Fryer, C. L., Woosley, S. E., Herant, M., & Davies, M. B. 1999, ApJ, 520, 650, doi: [10.1086/307467](https://doi.org/10.1086/307467)

Galama, T. J., Vreeswijk, P. M., van Paradijs, J., et al. 1998, Nature, 395, 670, doi: [10.1038/27150](https://doi.org/10.1038/27150)

Gao, H.-X., Geng, J.-J., Liang, Y.-F., et al. 2025, ApJ, 986, 106, doi: [10.3847/1538-4357/adceb1](https://doi.org/10.3847/1538-4357/adceb1)

Garcia-Cifuentes, K., Becerra, R., & De Colle, F. 2024, The Journal of Open Source Software, 9, 5923, doi: [10.21105/joss.05923](https://doi.org/10.21105/joss.05923)

Ghirlanda, G., Bernardini, M. G., Calderone, G., & D'Avanzo, P. 2015, Journal of High Energy Astrophysics, 7, 81, doi: [10.1016/j.jheap.2015.04.002](https://doi.org/10.1016/j.jheap.2015.04.002)

Ghirlanda, G., Salafia, O. S., Pescalli, A., et al. 2016, A&A, 594, A84, doi: [10.1051/0004-6361/201628993](https://doi.org/10.1051/0004-6361/201628993)

Gottlieb, O., Bromberg, O., Levinson, A., & Nakar, E. 2021, MNRAS, 504, 3947, doi: [10.1093/mnras/stab1068](https://doi.org/10.1093/mnras/stab1068)

Gottlieb, O., Bromberg, O., Singh, C. B., & Nakar, E. 2020, MNRAS, 498, 3320, doi: [10.1093/mnras/staa2567](https://doi.org/10.1093/mnras/staa2567)

Gottlieb, O., Lalakos, A., Bromberg, O., Liska, M., & Tchekhovskoy, A. 2022, MNRAS, 510, 4962, doi: [10.1093/mnras/stab3784](https://doi.org/10.1093/mnras/stab3784)

Gottlieb, O., Metzger, B. D., Quataert, E., et al. 2023, ApJL, 958, L33, doi: [10.3847/2041-8213/ad096e](https://doi.org/10.3847/2041-8213/ad096e)

Guetta, D., & Della Valle, M. 2007, ApJL, 657, L73, doi: [10.1086/511417](https://doi.org/10.1086/511417)

Guetta, D., & Piran, T. 2006, A&A, 453, 823, doi: [10.1051/0004-6361:20054498](https://doi.org/10.1051/0004-6361:20054498)

Halevi, G., Wu, B., Mösta, P., et al. 2023, ApJL, 944, L38, doi: [10.3847/2041-8213/acb702](https://doi.org/10.3847/2041-8213/acb702)

Hao, J.-M., & Yuan, Y.-F. 2013, A&A, 558, A22, doi: [10.1051/0004-6361/201321471](https://doi.org/10.1051/0004-6361/201321471)

Harrison, R., Gottlieb, O., & Nakar, E. 2018, MNRAS, 477, 2128, doi: [10.1093/mnras/sty760](https://doi.org/10.1093/mnras/sty760)

Hasan, A. M., & Azzam, W. J. 2024, International Journal of Astronomy and Astrophysics, 14, 20, doi: [10.4236/ijaa.2024.141002](https://doi.org/10.4236/ijaa.2024.141002)

Hirschi, R., Meynet, G., & Maeder, A. 2005, A&A, 443, 581, doi: [10.1051/0004-6361:20053329](https://doi.org/10.1051/0004-6361:20053329)

Hjorth, J., & Bloom, J. S. 2012, Gamma-ray bursts

Hjorth, J., Sollerman, J., Møller, P., et al. 2003, Nature, 423, 847, doi: [10.1038/nature01750](https://doi.org/10.1038/nature01750)

Kaneko, Y., Bostancı, Z. F., Göögüs, E., & Lin, L. 2015, MNRAS, 452, 824, doi: [10.1093/mnras/stv1286](https://doi.org/10.1093/mnras/stv1286)

Kasliwal, M. M., Nakar, E., Singer, L. P., et al. 2017, Science, 358, 1559, doi: [10.1126/science.aap9455](https://doi.org/10.1126/science.aap9455)

Khatiya, N. S., Dainotti, M. G., Narendra, A., et al. 2025, ApJ, 990, 69, doi: [10.3847/1538-4357/adf219](https://doi.org/10.3847/1538-4357/adf219)

Kouveliotou, C., Meegan, C. A., Fishman, G. J., et al. 1993, ApJL, 413, L101, doi: [10.1086/186969](https://doi.org/10.1086/186969)

Le, T., & Mehta, V. 2017, ApJ, 837, 17, doi: [10.3847/1538-4357/aa5fa7](https://doi.org/10.3847/1538-4357/aa5fa7)

Le, T., Ratke, C., & Mehta, V. 2020, MNRAS, 493, 1479, doi: [10.1093/mnras/staa366](https://doi.org/10.1093/mnras/staa366)

Lee, C.-H. 2010, Journal of Korean Physical Society, 56, 1619, doi: [10.3938/jkps.56.1619](https://doi.org/10.3938/jkps.56.1619)

Levan, A. J., Gompertz, B. P., Salafia, O. S., et al. 2024, Nature, 626, 737, doi: [10.1038/s41586-023-06759-1](https://doi.org/10.1038/s41586-023-06759-1)

Levan, A. J., Martin-Carrillo, A., Laskar, T., et al. 2025, ApJL, 990, L28, doi: [10.3847/2041-8213/adf8e1](https://doi.org/10.3847/2041-8213/adf8e1)

Lloyd-Ronning, N. 2022, The Astrophysical Journal, 928, 104, doi: [10.3847/1538-4357/ac54b3](https://doi.org/10.3847/1538-4357/ac54b3)

Lloyd-Ronning, N., Johnson, J., Cheng, R. M., et al. 2023, ApJ, 947, 85, doi: [10.3847/1538-4357/acc795](https://doi.org/10.3847/1538-4357/acc795)

Lloyd-Ronning, N. M., Aykutalp, A., & Johnson, J. L. 2019, MNRAS, 488, 5823, doi: [10.1093/mnras/stz2155](https://doi.org/10.1093/mnras/stz2155)

Lloyd-Ronning, N. M., Johnson, J., Upton Sanderbeck, P., Silva, M., & Cheng, R. M. 2024, MNRAS, 535, 2800, doi: [10.1093/mnras/staa2502](https://doi.org/10.1093/mnras/staa2502)

Lloyd-Ronning, N. M., Johnson, J. L., & Aykutalp, A. 2020, MNRAS, 498, 5041, doi: [10.1093/mnras/staa2787](https://doi.org/10.1093/mnras/staa2787)

Luo, J.-W., Wang, F.-F., Zhu-Ge, J.-M., et al. 2023, ApJ, 959, 44, doi: [10.3847/1538-4357/ad03ec](https://doi.org/10.3847/1538-4357/ad03ec)

Lyman, J. D., Levan, A. J., Tanvir, N. R., et al. 2017, MNRAS, 467, 1795, doi: [10.1093/mnras/stx220](https://doi.org/10.1093/mnras/stx220)

Lynden-Bell, D. 1971, MNRAS, 155, 95, doi: [10.1093/mnras/155.1.95](https://doi.org/10.1093/mnras/155.1.95)

MacFadyen, A. I., & Woosley, S. E. 1999, *ApJ*, 524, 262, doi: [10.1086/307790](https://doi.org/10.1086/307790)

Maoz, D., & Nakar, E. 2024, arXiv e-prints, arXiv:2406.08630, doi: [10.48550/arXiv.2406.08630](https://doi.org/10.48550/arXiv.2406.08630)

—. 2025, *ApJ*, 982, 179, doi: [10.3847/1538-4357/ada3bd](https://doi.org/10.3847/1538-4357/ada3bd)

Matzner, C. D. 2003, *MNRAS*, 345, 575, doi: [10.1046/j.1365-8711.2003.06969.x](https://doi.org/10.1046/j.1365-8711.2003.06969.x)

Metzger, B. D., Quataert, E., & Thompson, T. A. 2008, *MNRAS*, 385, 1455, doi: [10.1111/j.1365-2966.2008.12923.x](https://doi.org/10.1111/j.1365-2966.2008.12923.x)

Moharana, R., & Piran, T. 2017, *MNRAS*, 472, L55, doi: [10.1093/mnrasl/slx131](https://doi.org/10.1093/mnrasl/slx131)

Moss, M., Lien, A., Guiriec, S., Cenko, S. B., & Sakamoto, T. 2022, *ApJ*, 927, 157, doi: [10.3847/1538-4357/ac4d94](https://doi.org/10.3847/1538-4357/ac4d94)

Nakar, E., Gal-Yam, A., & Fox, D. B. 2006, *ApJ*, 650, 281, doi: [10.1086/505855](https://doi.org/10.1086/505855)

Nakar, E., & Piran, T. 2002, *MNRAS*, 331, 40, doi: [10.1046/j.1365-8711.2002.05158.x](https://doi.org/10.1046/j.1365-8711.2002.05158.x)

Narayan, R., Paczynski, B., & Piran, T. 1992, *ApJL*, 395, L83, doi: [10.1086/186493](https://doi.org/10.1086/186493)

Negro, M., Cibrario, N., Burns, E., et al. 2024, Prompt GRB recognition through waterfalls and deep learning, arXiv:2406.03643 [astro-ph.IM]. <https://arxiv.org/abs/2406.03643>

O'Connor, B., Beniamini, P., Troja, E., et al. 2025, arXiv e-prints, arXiv:2509.07141, doi: [10.48550/arXiv.2509.07141](https://doi.org/10.48550/arXiv.2509.07141)

Perley, D. A., Krühler, T., Schulze, S., et al. 2016, *ApJ*, 817, 7, doi: [10.3847/0004-637X/817/1/7](https://doi.org/10.3847/0004-637X/817/1/7)

Petrosian, V., & Dainotti, M. G. 2024, *ApJL*, 963, L12, doi: [10.3847/2041-8213/ad2763](https://doi.org/10.3847/2041-8213/ad2763)

Petrosian, V., Kitanidis, E., & Kocevski, D. 2015, *ApJ*, 806, 44, doi: [10.1088/0004-637X/806/1/44](https://doi.org/10.1088/0004-637X/806/1/44)

Piran, T. 1992, *ApJL*, 389, L45, doi: [10.1086/186345](https://doi.org/10.1086/186345)

—. 2004, *Reviews of Modern Physics*, 76, 1143, doi: [10.1103/RevModPhys.76.1143](https://doi.org/10.1103/RevModPhys.76.1143)

Rastinejad, J. C., Gompertz, B. P., Levan, A. J., et al. 2022, *Nature*, 612, 223, doi: [10.1038/s41586-022-05390-w](https://doi.org/10.1038/s41586-022-05390-w)

Ristić, M., Barker, B. L., Cupp, S., et al. 2025, arXiv e-prints, arXiv:2509.03003, doi: [10.48550/arXiv.2509.03003](https://doi.org/10.48550/arXiv.2509.03003)

Rossi, A., Rothberg, B., Palazzi, E., et al. 2022, *ApJ*, 932, 1, doi: [10.3847/1538-4357/ac60a2](https://doi.org/10.3847/1538-4357/ac60a2)

Santoliquido, F., Mapelli, M., Artale, M. C., & Boco, L. 2022, *MNRAS*, 516, 3297, doi: [10.1093/mnras/stac2384](https://doi.org/10.1093/mnras/stac2384)

Soderberg, A. M., Kulkarni, S. R., Nakar, E., et al. 2006, *Nature*, 442, 1014, doi: [10.1038/nature05087](https://doi.org/10.1038/nature05087)

Tanvir, N. R., Laskar, T., Levan, A. J., et al. 2018, *ApJ*, 865, 107, doi: [10.3847/1538-4357/aadba9](https://doi.org/10.3847/1538-4357/aadba9)

Troja, E., Fryer, C. L., O'Connor, B., et al. 2022, *Nature*, 612, 228, doi: [10.1038/s41586-022-05327-3](https://doi.org/10.1038/s41586-022-05327-3)

Tsvetkova, A., Frederiks, D., Golenetskii, S., et al. 2017, *ApJ*, 850, 161, doi: [10.3847/1538-4357/aa96af](https://doi.org/10.3847/1538-4357/aa96af)

Urrutia, G., Janiuk, A., & Olivares, H. 2025, arXiv e-prints, arXiv:2507.10231, doi: [10.48550/arXiv.2507.10231](https://doi.org/10.48550/arXiv.2507.10231)

Wanderman, D., & Piran, T. 2015, *MNRAS*, 448, 3026, doi: [10.1093/mnras/stv123](https://doi.org/10.1093/mnras/stv123)

Wang, F., Zou, Y.-C., Liu, F., et al. 2020, *ApJ*, 893, 77, doi: [10.3847/1538-4357/ab0a86](https://doi.org/10.3847/1538-4357/ab0a86)

Woosley, S., & Bloom, J. 2006, *Annu. Rev. Astron. Astrophys.*, 44, 507

Woosley, S. E., & Heger, A. 2006, *ApJ*, 637, 914, doi: [10.1086/498500](https://doi.org/10.1086/498500)

Yang, J., Ai, S., Zhang, B.-B., et al. 2022, *Nature*, 612, 232, doi: [10.1038/s41586-022-05403-8](https://doi.org/10.1038/s41586-022-05403-8)

Yang, Y.-H., Troja, E., O'Connor, B., et al. 2024, *Nature*, 626, 742, doi: [10.1038/s41586-023-06979-5](https://doi.org/10.1038/s41586-023-06979-5)

Yoon, S.-C., & Langer, N. 2005, *A&A*, 443, 643, doi: [10.1051/0004-6361:20054030](https://doi.org/10.1051/0004-6361:20054030)

Yoon, S.-C., Langer, N., & Norman, C. 2006, *A&A*, 460, 199, doi: [10.1051/0004-6361:20065912](https://doi.org/10.1051/0004-6361:20065912)

Yu, H., Wang, F. Y., Dai, Z. G., & Cheng, K. S. 2015, *ApJS*, 218, 13, doi: [10.1088/0067-0049/218/1/13](https://doi.org/10.1088/0067-0049/218/1/13)

Zevin, M., Nugent, A. E., Adhikari, S., et al. 2022, *ApJL*, 940, L18, doi: [10.3847/2041-8213/ac91cd](https://doi.org/10.3847/2041-8213/ac91cd)

Zhang, H.-M., Huang, Y.-Y., Zheng, J.-H., Liu, R.-Y., & Wang, X.-Y. 2022, *ApJL*, 933, L22, doi: [10.3847/2041-8213/ac7b23](https://doi.org/10.3847/2041-8213/ac7b23)

Zhu, J.-P., Wang, X. I., Sun, H., et al. 2022, *ApJL*, 936, L10, doi: [10.3847/2041-8213/ac85ad](https://doi.org/10.3847/2041-8213/ac85ad)

Zhu, S.-Y., Sun, W.-P., Ma, D.-L., & Zhang, F.-W. 2024, arXiv e-prints, arXiv:2406.05357, <https://arxiv.org/abs/2406.05357>

APPENDIX

1. Redshift Evolution of the Distribution

Figure 6 shows the intrinsic duration distributions, separated into “low” redshift (blue lines) and “high” redshift (orange lines) sub-samples for different values of the redshift delimiter, ranging from $2 \lesssim (1+z) \lesssim 4.5$. It is clear that separating the sample at a redshift that falls between $(1+z) \sim 2$ to $(1+z) \sim 3$ shows a clear difference in the dN/dT distributions, in that a plateau is present in the high redshift sample, but not in the low redshift sample. If sample biases and completeness are not playing too large of a role in these distributions, this would indicate non-collapsar progenitors begin to dominate the GRB distribution below redshifts of about $(1+z) \sim 2$, while there is a clear signature of the collapsar progenitor above this redshift.

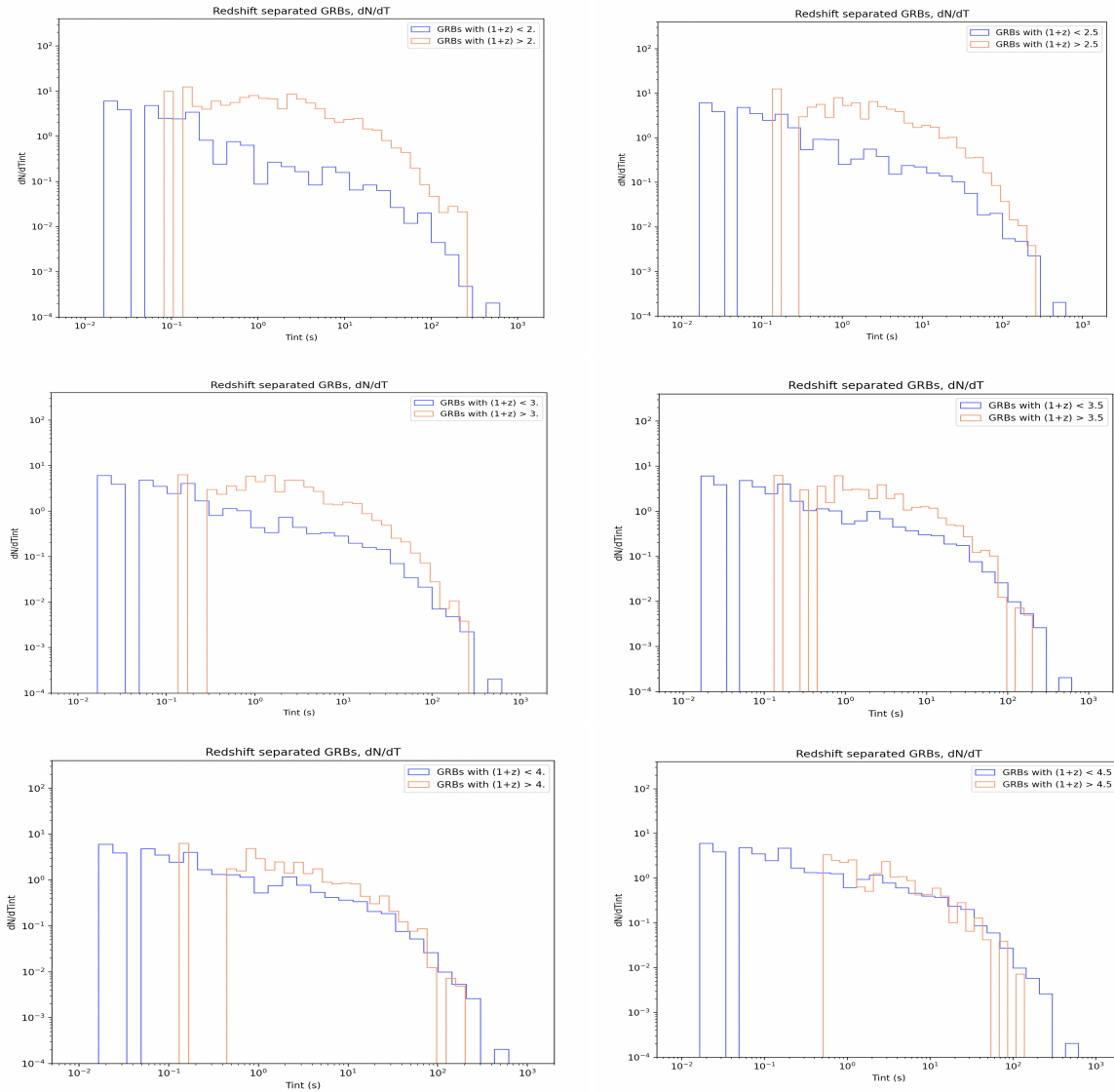


Figure 6. Evolution of the redshift separated dN/dT_{int} distribution for different values of the delimiting redshift, with “low” redshift are shown by blue lines and “high” redshift are showing by orange lines.

2. Hard/Soft Division

Figure 7 shows the single power-law (right panel) and cutoff power-law (left panel) spectral indices, defined in equations 2 and 3 respectively, as a function of T_{90} for *Swift* GRBs. A higher α indicates a softer burst. The traditional long-soft/short-hard separation is apparent. Hence anything above the upper line in either figure is what we define as a “soft” burst. Anything below the lower line in either figure is what we call a “hard” burst.

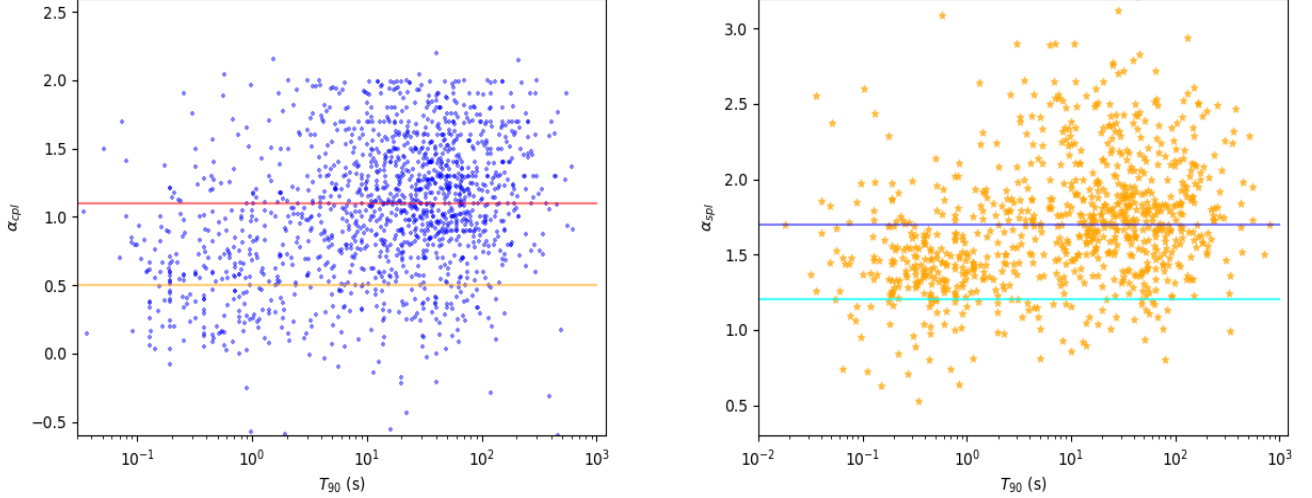


Figure 7. Photon spectrum power law index vs T_{90} for a cutoff power-law model (left panel) and a single power-law model (right panel). Above the upper lines defines our soft sample for each model; below the lower lines defines our hard sample.

3. Additional Progenitor and Jet Parameter Space

Below, we provide additional contour plots of the threshold time calculated in section 4.3, for a broader range of jet and progenitor properties than shown in the main text in Figure 5, where we used the average observed jet luminosity and opening angle values from our high redshift sample in our calculations. Following our display in the main text, for each of the plots in Figure 8, the left panels show the calculation according to equation 4, while the right panels show this timescale with a numerical correction applied according to the simulations of Harrison et al. (2018).

The top panels show the threshold time for a $40M_{\odot}$ star (with all other variables as in the main text), the middle panels show the jet threshold time for a jet luminosity one tenth of the average observed value, and the bottom panels show the threshold time for a jet opening angle half of the average observed value. As in the main text the black dotted and solid lines show a threshold time of 5 seconds and 15 seconds, respectively.

As expected, a larger progenitor mass will increase the threshold time, as will a lower luminosity jet. Meanwhile, a smaller opening angle will decrease the time it takes the jet to propagate through the star and therefore requires larger progenitor radii to be consistent with the plateau end timescale.

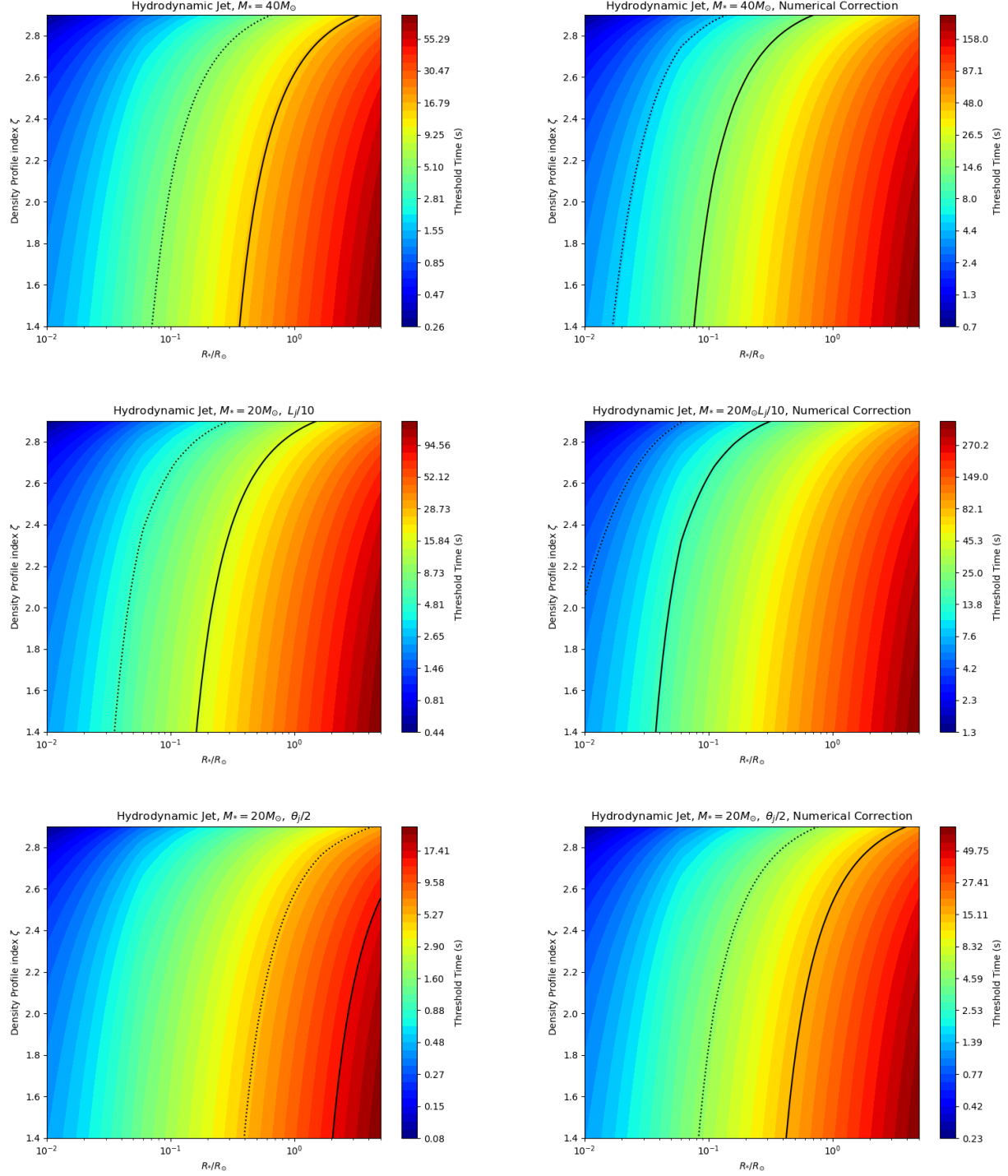


Figure 8. Threshold time for different progenitor masses, jet luminosity and jet opening angle. the left panels show the calculation according to equation 4, while the right panels show this timescale with a numerical correction applied according to the simulations of Harrison et al. (2018). The top panels show the threshold time for a $40M_{\odot}$ star (with all other variables as in the main text), the middle panels show the threshold time for a jet luminosity $L_j = 2 \times 10^{49}$ erg/s, one tenth of the average observed value of our high redshift sample, and the bottom panels show the threshold time for a jet opening angle $\theta_o = 2.9^\circ$ half of the average observed value of our high redshift sample.